

# Multi-Frequency Channel Modeling for Millimeter Wave and THz Wireless Communication via Generative Adversarial Networks

Yaqi Hu, Mingsheng Yin, William Xia, Sundeep Rangan, Marco Mezzavilla  
NYU Tandon School of Engineering, Brooklyn, NY, USA

**Abstract**—Modern cellular systems rely increasingly on simultaneous communication in multiple discontinuous bands for macro-diversity and increased bandwidth. Multi-frequency communication is particularly crucial in the millimeter wave (mmWave) and Terahertz (THz) frequencies, as these bands are often coupled with lower frequencies for robustness. Evaluation of these systems requires statistical models that can capture the joint distribution of the channel paths across multiple frequencies. This paper presents a general neural network based methodology for training multi-frequency double directional statistical channel models. In the proposed approach, each is described as a multi-clustered set, and a generative adversarial network (GAN) is trained to generate random multi-cluster profiles where the generated cluster data includes the angles and delay of the clusters along with the vectors of random received powers, angular, and delay spread at different frequencies. The model can be readily applied for multi-frequency link or network layer simulation. The methodology is demonstrated on modeling urban micro-cellular links at 28 and 140 GHz trained from extensive ray tracing data. The methodology makes minimal statistical assumptions and experiments show the model can capture interesting statistical relationships between frequencies.

**Index Terms**—Channel modeling, millimeter wave, sub-terahertz, neural networks, GANs

## I. INTRODUCTION

Cellular wireless systems often operate over multiple frequency bands simultaneously for increased bandwidth and macro-diversity. Commercial cellular system support several mechanisms for multi-band operation including carrier aggregation [1], dual connectivity [2], and multi-connectivity [3]. The simultaneous use of multiple frequencies is particularly important in the millimeter wave (mmWave) and terahertz (THz) bands where lower frequency carriers are needed for robustness and control signaling [4], [5]. There has also been active research in leveraging information from lower frequencies for communication in the mmWave and THz bands for procedures such as beam search [6], [7], [8], and localization and sensing [9].

Evaluation of these systems, necessitates channel models that can describe the behavior of links across multiple frequency bands. In this work, we seek to develop *statistical*

*channel models* that can generate random instances of the channel parameters following the observed statistical distribution of channel parameters in some environment (e.g. urban micro). Statistical models such as those by 3GPP [10] are the mainstay for commercial cellular evaluation and are a critical initial step in any simulation evaluation.

Developing accurate statistical channel models for mmWave systems is well known to be challenging, even for a single band. Since mmWave systems operate at very high bandwidths with highly directional beams, statistical models must capture the full *double directional* nature of the channel meaning the angles of arrival and departure, delays and gains of all the paths [11]. This difficulty is compounded in the multi-frequency setting, where one must generate gains of the paths across multiple frequencies. These parameters can have complex relationships as factors that influence propagation, such as transmission and reflection losses, vary considerably across frequency [12].

Due to the difficulty in modeling wireless channels from first principles, there has been a growing interest in using data driven, neural networks (NN) based techniques [13], [14], [15], [16], [17], [18]. The key benefit of these approaches is that they make minimal assumptions and can thus learn complex statistical relationships between variables. In this line, the work in [18] used NNs for air-to-ground channel models at 28 GHz. The approach was able to model the full double-directional nature of the channel and demonstrated the ability to learn non-obvious relationships. In addition, the trained models considerably outperformed standard 3GPP models such as [10], which assume very specific structures to be tractable.

In this work, we wish to model the *joint* distribution of the paths between a transmitter (TX) and receiver (RX) across multiple frequencies. The channel is modeled by a set of clusters and a generative model is then used to generate the cluster parameters from the distance between the TX and RX. The paper then develops and evaluates several new features as compared to the modelling methodology of [18] to support multiple frequencies:

- *Multi-frequency cluster models*: Most importantly, the model represents the channel in a compact manner that can capture the key commonalities and differences between frequencies. Specifically, the channel is represented by a set of clusters whose mean angles of arrivals and

The authors were supported by NSF grants 1952180, 1925079, 1564142, 1547332, the SRC, OPPO, and the industrial affiliates of NYU WIRELESS. The work was also supported by Remcom that provided the Wireless Insite software.

departure and delay are common among the frequencies, reflecting that macro-level path of propagation are not frequency dependent. On the other hand, the power, and the angular and delay spread are modeled as frequency dependent to capture the variations in scattering and transmission losses across the frequencies, which is particularly vital to model in the mmWave and THz regimes [19], [20], [21], [22].

- *Ray tracing processing:* There are limited number of multi-frequency channel measurements [23], [24] and these generally have an insufficient numbers of data points for training large NNs. Similar to [18], [25], [26], we thus employ a powerful ray tracing package, Wireless InSite by Remcom [27], to obtain high volume training data.
- *Cluster identification and pre-processing:* When using the ray tracing data, we propose a novel clustering algorithm as a pre-processing step that identifies common clusters across frequencies but captures the delay and angular variations in different frequencies. The methods can be considered as a multi-frequency extension of clustering techniques proposed in [28].
- *Evaluation on micro-cellular urban environment:* The method is evaluated on micro-cellular terrestrial links in a region ( $\approx 0.6 \times 0.4$  km<sup>2</sup>) of Beijing, China. It is shown that the method can capture important correlations in the channel characteristics between frequencies.

## II. MULTI-FREQUENCY MODELING PROBLEM

We consider the modeling of channels on  $M$  frequencies,  $f_1, \dots, f_M$ . For example, in the examples below, we will look at two frequencies:  $f_1 = 28$  GHz and  $f_2 = 140$  GHz. We model a single link, meaning the channel from a transmitter (TX) to receiver (RX). For the cellular applications below, the TX will be the base station (gNB) and the RX will be the mobile user equipment (UE). However, due to reciprocity, the TX and RX can be reversed. We model the channel across the  $M$  frequencies by a common set of  $L$  clusters where each cluster  $\ell$  is described by a vector of parameters,

$$\mathbf{x}^{(\ell)} = [\tilde{\tau}_\ell, \bar{\theta}_\ell^{\text{rx}}, \bar{\phi}_\ell^{\text{rx}}, \bar{\theta}_\ell^{\text{tx}}, \bar{\phi}_\ell^{\text{tx}}, F_{\ell 1}, \dots, F_{\ell M}], \quad (1)$$

where  $\tilde{\tau}_\ell$  is the minimum path delay within the cluster,  $\bar{\theta}_\ell^{\text{rx}}, \bar{\phi}_\ell^{\text{rx}}$  are the average intra-cluster inclination and azimuth angles of arrival (AoA),  $\bar{\theta}_\ell^{\text{tx}}, \bar{\phi}_\ell^{\text{tx}}$  are the average intra-cluster inclination and azimuth angles of departure (AoD). These parameters are common across the clusters, reflecting that the angles and delay are dependent on the large scale path routes and do not depend on the frequency. In contrast, the parameters  $F_{\ell m}, m = 1, \dots, M$ , are the frequency-dependent components given by

$$F_{\ell m} = [\Delta\theta_{\ell m}^{\text{rx}}, \Delta\phi_{\ell m}^{\text{rx}}, \Delta\theta_{\ell m}^{\text{tx}}, \Delta\phi_{\ell m}^{\text{tx}}, \Delta\tau_{\ell m}, P_{\ell m}], \quad (2)$$

where  $\Delta\theta_{\ell m}^{\text{rx}}, \Delta\phi_{\ell m}^{\text{rx}}$  are root mean square (RMS) inclination and azimuth angles of arrival spread,  $\Delta\theta_{\ell m}^{\text{tx}}, \Delta\phi_{\ell m}^{\text{tx}}$  are the RMS inclination and azimuth angles of departure spread,  $\Delta\tau_{\ell m}$  is the RMS delay spread,  $P_{\ell m}$  is the total received

power. The multi-frequency channel can then be described by the set of  $L$  clusters

$$\mathbf{x} = [\mathbf{x}^{(1)}, \dots, \mathbf{x}^{(L)}]. \quad (3)$$

We will call  $\mathbf{x}$  the *cluster vector*.

To simplify the modeling, we will fix the number of clusters at  $L = 10$ . When there are less than  $L$  clusters at a certain frequency, say  $L_0 < L$ , we simply set  $P_{\ell m} = 0$  (in linear scale) for all  $\ell > L_0$  at frequency  $m$ . Similarly, if a path cluster exist in one frequency  $m$  but not at another frequency  $m'$ , we take  $P_{\ell m} > 0$  and  $P_{\ell m'} = 0$ . This scenario can occur, for example, where a path can penetrate materials at a lower frequency, but be blocked at a millimeter wave frequency.

The above parameterization captures the fact that the geometric path route is independent of frequency. However, the angular spread from scattering as well as the transmission and reflection losses are well-known to be frequency dependent – for example, see the scattering studies in THz in [19], [20], [21]. We also note that the 3GPP procedure for multi-frequency models also generates paths with common cluster mean angles of arrival and departure, but frequency dependent gains and angular spread [10]. However, the frequency-dependent components are assumed to be independent in the 3GPP model. In contrast, our procedure is general and can, in principle, learn statistical relationships with sufficient data.

Since the model (1) has  $5 + 6M$  parameters per cluster, and  $L$  clusters, there are a total of  $(5 + 6M)L$  parameters in (3). For example, in the example below, we will consider  $M = 2$  frequencies and  $L = 10$  clusters for a total of  $p = (5 + 6M)L = 170$  parameters.

Each link also has a condition vector,  $\mathbf{u}$ . For our case, we will simply take

$$\mathbf{u} = (d_x, d_y, d_z), \quad (4)$$

the 3D vector between the TX and RX. Other parameters could be added to  $\mathbf{u}$  such as the antenna heights or cell types.

The statistical channel modeling problem is to model the distribution of the cluster vector  $\mathbf{x}$  as a function of the link conditions  $\mathbf{u}$ . That is, we want to model the conditional probability distribution  $p(\mathbf{x}|\mathbf{u})$ . In this work, we will be interested in so-called generative models where the conditional distribution is represented as a mapping

$$\mathbf{x} = g(\mathbf{u}, \mathbf{z}), \quad (5)$$

where  $\mathbf{z}$  is some random vector with a known distribution.

Generative models (5) are the basis for cellular evaluations such as [10]. For example, the gNBs and UEs are first randomly placed in an environment following some deployment model assumption (e.g. urban micro with some inter-site distance and density). The deployment determines the link conditions  $\mathbf{u}$  between each gNB and UE. Using a generative model (5), we can then randomly generate path parameters between all the gNBs and UEs. Once we combine these path parameters with the antenna array assumptions on both sides, we can determine all the MIMO channels in the network. One can then run any algorithm of interest to evaluate

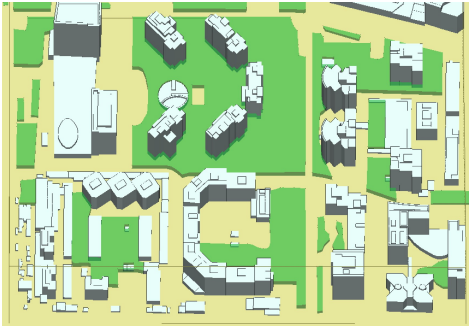


Fig. 1. Ray tracing simulation area representing a  $550 \times 380$  m<sup>2</sup> region of Beijing, China.

relevant system performance statistics such as the SNR or rate distribution.

### III. URBAN CELLULAR RAY TRACING DATA AND SCATTERING MODELING

Although our methodology is general, we will demonstrate the methods on two frequencies:  $f_1 = 28$  GHz, as used in 5G systems today [29], and  $f_2 = 140$  GHz, a key sub-THz frequency targeted for potential 6G use cases [30], [31]. While there have been recent multi-frequency measurement campaigns [23], [24], these measurements are enormously time-consuming and there are no current datasets with sufficient data points for training complex neural networks. Thus, similar to several recent works [18], [26], [25] we use a powerful ray tracing tool, Wireless InSite by Remcom [27] to generate data for training. Specifically, an area of Beijing, China, consisting of  $550 \times 380$  square meters as shown in Fig. 1, is imported. Using similar parameters to 3GPP report [10], we manually place 100 terrestrial receiving gNBs on the outside of buildings with 10 m height, and transmitting UEs are placed at 320 locations on streets 1.5 m. The deployment results in  $100 \times 320 = 32000$  links (i.e. gNB-UE pairs). We run independent ray tracing simulations on these the two frequencies. We set the maximum number of reflections as six and the maximum number of diffraction as one, and we limited the maximum number of paths of a link to 20. In addition, the ray tracing tool only collects paths with a power of at least -250 dBm.

Critical to modeling the frequency dependence is the effect of diffuse scattering, which is particularly prominent in the mmWave and THz frequencies [20], [21], [22]. As part of our simulation, we enable the diffusing scattering model in the ray tracing tool which is based on the directive model developed by [19]. A key parameter is the scattering coefficient,  $S$ , which is the ratio of the scattered to incident electric field. Following measurements in [19], we set the scattering coefficient to  $S = 0.273$  for 28 GHz, and  $S = 0.4$  for 140 GHz, in which case, rays in 140 GHz disperse more power on the forward lobe of diffuse scattered. A diffuse scattering interaction is limited to the last interaction along a path before it reaches the receiver. This helps reduce the run time for diffuse scattering calculations.

## IV. PATHS CLUSTER AND GENERATIVE NEURAL NETWORK MODELING

### A. Path Clusters Identification by $K$ -means

The ray tracing data produces rays at each frequency. Our first step is to pre-process the rays to identify the clusters and determine the cluster parameters. Similar to [28], we use a  $k$ -means clustering procedure on the inclination and azimuth angles of arrival, inclination and azimuth angles of departure, and delay for each link of the set. Silhouette scores [32] are used to determine the best number of clusters for each link. A typical identification of the clusters is shown in the map in (2) where the circles indicate the identified clusters.

After identifying the clusters, we can determine the angular and delay spread and power in each cluster to generate the cluster vector  $\mathbf{x}$  as indicated in (3) for each link. To limit the size of the cluster vector, we use  $L = 10$  as the maximum number of clusters.

We obtain one data record  $\mathbf{x}$  for each link. Each link also has condition vector  $\mathbf{u}$  as in (4). The condition vector  $\mathbf{u}$  is first converted to a 3D distance and the logarithm of the 3D distance, denoted  $\mathbf{u} = (d_{3D}, \log_{10} d_{3D})$ .

### B. Cluster Generative Network

The goal of the network is to generate random cluster vectors  $\mathbf{x}$  in (3) following the conditional distribution  $p(\mathbf{x}|\mathbf{u})$  as observed in the data. For this purpose, we use a conditional Wasserstein generative adversarial network with gradient penalty (CWGAN-GP) [33], [34] that is relatively simple to implement while being effective in complex datasets.

The CWGAN-GP can be summarized as follows: There are two components: a *generator*  $\mathbf{G}$  and *critic*  $\mathbf{C}$ . The generator takes the condition vector  $\mathbf{u}$  and some random input  $\mathbf{z} \sim p(\mathbf{z})$  and generates a random path data vector  $\mathbf{x} = \mathbf{G}(\mathbf{u}, \mathbf{z})$ . The vector  $\mathbf{z}$  is called the *latent vector*. As is commonly used, we take its distribution  $p(\mathbf{z})$  to be a unit variance Gaussian vector. We set the latent dimension to 20. To ensure the generator matches the data distribution, one also trains a critic function  $\mathbf{C}$  that attempt to discriminate between the generated and true samples. The critic  $\mathbf{C}$  and generator  $\mathbf{G}$  networks are trained via a loss:

$$L = \underbrace{\mathbb{E}_{\tilde{\mathbf{x}} \sim \mathbb{P}_g} [C(\tilde{\mathbf{x}})] - \mathbb{E}_{\mathbf{x} \sim \mathbb{P}_r} [C(\mathbf{x})]}_{\text{Original critic loss}} + \underbrace{\lambda \mathbb{E}_{\hat{\mathbf{x}} \sim \mathbb{P}_{\hat{\mathbf{x}}}} \left[ (\|\nabla_{\hat{\mathbf{x}}} D(\hat{\mathbf{x}})\|_2 - 1)^2 \right]}_{\text{Gradient penalty}}. \quad (6)$$

where  $\mathbb{P}_g$  is the generator distribution implicitly defined by  $\tilde{\mathbf{x}} = \mathbf{G}(\mathbf{u}, \mathbf{z})$ ,  $\mathbf{z} \sim p(\mathbf{z})$ , and  $\mathbb{P}_r$  is the distribution of the data points. The loss (6) is optimized via a minimax: The critic  $\mathbf{C}$  attempts to minimize the loss to discriminate between the generated and true samples, while the generators attempts to maximize the loss to fake the critic. The minimax is similar to other GANs, but the key concept in the WGAN-GP is that the gradient penalty term avoids mode collapse – see [33],

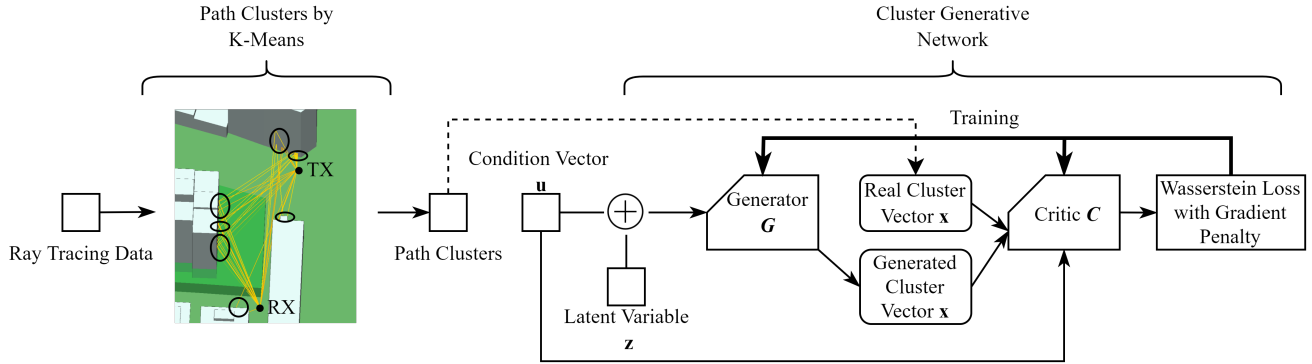


Fig. 2. The architecture for the K-Means path clusters generator and the generative adversarial neural network model

TABLE I  
GENERATIVE MODEL CONFIGURATION

	Cluster GAN Critic	Cluster GAN Generator
Num. of inputs	170 + 2	20 + 2
Hidden units	[1120,560,280]	[280,560,1120]
Num. of outputs	1	140
Optimizer	Adam	
Learning rate	0.0001	
Epochs	10000	
Batch size	1024	
Num. of parameters	1167551	1142290*

\*Different from the traditional parameters calculation method

[34] for details. For our application, both the generator and critic are realized with as fully connected neural networks with parameters shown in Table I.

One important detail for the wireless channel modeling is that the condition vector  $\mathbf{u}$  and cluster data  $\mathbf{x}$  have heterogeneous data types and need to be brought to a uniform format. To overcome this challenge, we align the angles of each path to the LOS direction and measure excess signal delay relative to the LOS distance delay. We then scale all the values using either min-max or standard scalers. Details are in the code [35].

## V. MODELING RESULTS

As described in Section III, the data consists of 32000 links, with each link having the paths at both 28 GHz and 140 GHz. We show the path clusters following on a GAN framework is able to capture interesting joint statistics between these two frequencies. In all the experiments below, we use 80% of the links for training and 20% for test. The generative network is implemented in Tensorflow 2, and the data set, code, and pre-train models can be accessed through [35].

### A. Received Power with Omnidirectional Antennas

We first evaluate the ability of the model to capture the joint distribution of the total received power at the two frequencies. The comparison can be performed as follows: Let  $\tilde{\mathbf{x}} = \mathbf{G}(\mathbf{u}, \mathbf{z})$  denote the learned generative model and

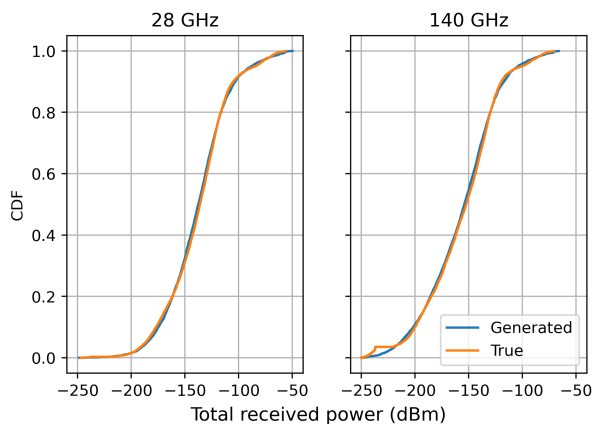


Fig. 3. The CDF of the total received power of links on the test data versus the CDF of randomly generated links' total received power from the trained model.

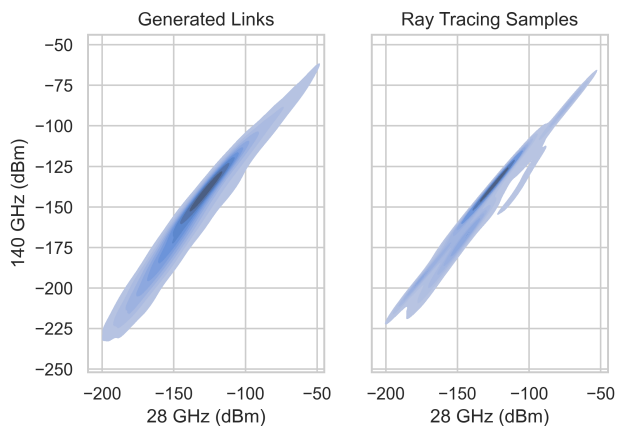


Fig. 4. The KDE plot of bivariate distributions of the total received power in 28 GHz and 140 GHz.

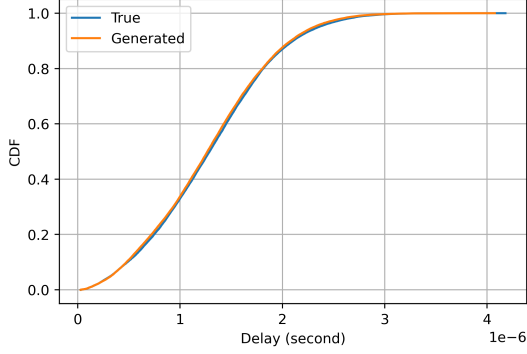


Fig. 5. The CDF of the paths minimum delay in clusters.

let  $(\mathbf{u}_i, \mathbf{x}_i)$ ,  $i = 1, \dots, N_{\text{ts}}$  denote the test data, where each sample contains the link condition  $\mathbf{u}_i$  and the corresponding cluster data vector  $\mathbf{x}_i$ . For each test sample, we can compute the vector

$$\mathbf{v}_i = (v_{i1}, v_{i2}) = (\phi_1(\mathbf{x}_1), \phi_2(\mathbf{x}_2)), \quad (7)$$

where  $v_{ij}$  is the omni-directional received power on sample  $i$  at frequency  $j$  where  $j = 1, 2$ . Here,  $\phi_j(\mathbf{x})$  is the function that computes the omni-directional received power at frequency  $j$  from the cluster data  $\mathbf{x}$ . The omni-directional received power is simply the received power that would be experienced if the gNB and UE had omni-directional antennas.

To compare these values with the generated distribution, for each test sample  $i$ , we also generate a random sample  $\mathbf{x}_i^{\text{rnd}} = \mathbf{G}(\mathbf{u}_i, \mathbf{z}_i)$  using the trained generator  $\mathbf{G}$  and a random  $\mathbf{z}_i$  with the same conditions  $\mathbf{u}_i$  as the test data. We can then compute a set of generated received powers

$$\mathbf{v}_i^{\text{rnd}} = (v_{i1}^{\text{rnd}}, v_{i2}^{\text{rnd}}) = (\phi_1(\mathbf{x}_1^{\text{rnd}}), \phi_2(\mathbf{x}_2^{\text{rnd}})), \quad (8)$$

Ideally, the samples  $\mathbf{v}_i$  and  $\mathbf{v}_i^{\text{rnd}}$  should have a similar distribution.

Fig. 3 plots the empirical cumulative distribution functions (CDFs) for the *marginal* distributions for the data and model at the two frequencies. Specifically, the left plot shows the CDF of the data  $v_{ij}$  and generated samples  $v_{ij}^{\text{rnd}}$  at frequency  $j = 1$ . The right plot shows the data and generated CDF for frequency  $j = 2$ . We see in both cases, these two marginal CDFs match almost perfectly.

But, what is most interesting is that the generator can also capture the joint statistics. The left panel of Fig. 4 shows a kernel density estimation (KDE) plot of the test data points  $(v_{i1}, v_{i2})$  and the right panel shows a KDE plot of the trained model  $(v_{i1}^{\text{rnd}}, v_{i2}^{\text{rnd}})$ . We see that the two *joint* distributions match well.

### B. Delay Distribution and RMS Delay Spread

To evaluate the model's ability to generate the delay, we first plot the CDF of the minimum path delay over the clusters, as shown in Fig. 5. There is an almost identical delay between clusters generated by the network and the real ray

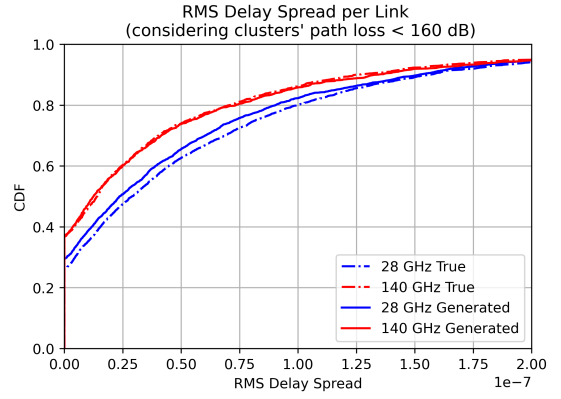


Fig. 6. The CDF of the RMS cluster delay spread per link, where we only considering the path loss of the clusters are smaller than 160 dB.

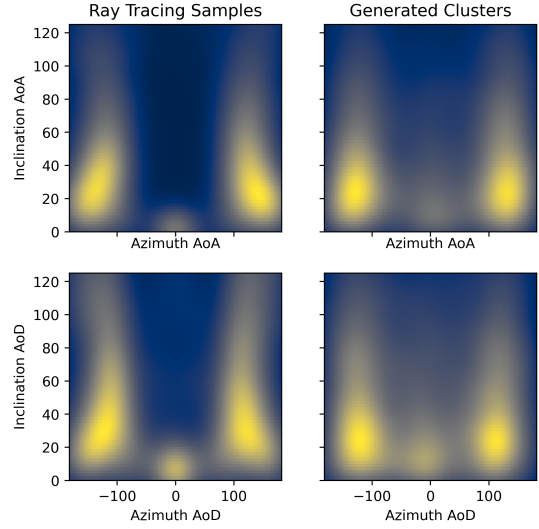


Fig. 7. Azimuth angles vs. inclination angles, where we only consider the path loss of the clusters that are smaller than 160 dB.

tracing value, and the maximum delay is also around 4000 nanoseconds. For each link, we also compute the RMS delay spread in order to gain an intuitive understanding of how the model fits the delays across the different clusters within a link. Fig. 6 shows that the RMS delay spread at 140 GHz is smaller than at 28 GHz overall. As the frequency increases, the RMS delay spread becomes smaller due to the increase in power loss by diffuse scattering. This conclusion is consistent with the mmWave and sub-Terahertz measurements in [22].

### C. Angles Distribution and RMS Angles Spread

As we mentioned above, to overcome the challenge of heterogeneous data types, we align the angles of each path to the direction of LOS. More precisely, when preprocessing the angles of arrival, we choose the LOS AoA direction of a link as the z-axis of the new spherical coordinate system and calculate the associated azimuth and inclination transformation angles.

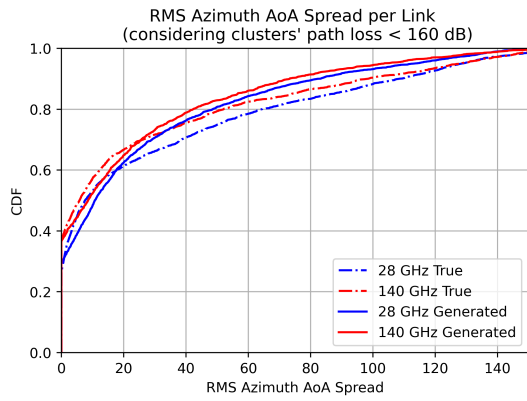


Fig. 8. RMS azimuth AoA spread, including the zero values.

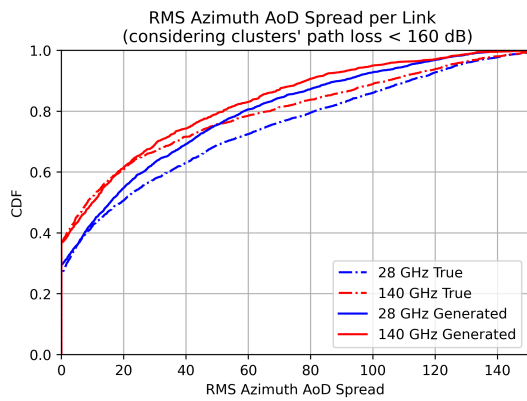


Fig. 9. RMS azimuth AoD spread, including the zero values.

Similarly, in the case of angles of departure, the AoD direction of LOS is used. In this way, the network can more effectively learn a statistical model of the angle relative to the condition vector. As illustrated in Fig.7, both AoA and AoD distributions are similar to those observed in real ray tracing samples. On the other hand, the RMS angle spread has important implications for evaluating channel models, especially when considering mmWave and sub-Terahertz bands. Fig.8 and Fig.9 show CDF images of AoA and AoD RMS spread, respectively. Overall, the model is able to capture the properties of the RMS angle spread at both frequencies. As a result of our testing, the RMS angle spread at 28 GHz is slightly greater than at 140 GHz. When there is only one cluster on a link at a given frequency, the RMS angle spread is zero. Based on Figs. 8 and 9, we can see that at 140 GHz, the proportion of RMS spread value of zero is higher than that at 28 GHz, owing to higher diffuse scattered power and increased path loss, which reduces the number of paths that can be detected by the receiver. The above observations are consistent with the conclusions obtained from actual measurements at 28 GHz and 140 GHz in [22].

## VI. CONCLUSION

Wireless multi-path channels can exhibit complex statistical relationships across different frequencies which are difficult to capture via standard models such as [10], particularly for mmWave and THz channels. In this work, we have presented a general modeling methodology for deriving full double directional models at multiple frequencies. The methods use state-of-the-art neural networks and make minimal a priori assumptions in the data. As such, we show they are able to capture interesting cross-frequency relations. The current method is based on extensive ray tracing data. A natural extension, left as future work, will be to augment the data with real data as these become available.

## REFERENCES

- [1] Z. Shen, A. Papasakellariou, J. Montojo, D. Gerstenberger, and F. Xu, "Overview of 3GPP LTE-Advanced Carrier Aggregation for 4G Wireless Communications," *IEEE Communications Magazine*, vol. 50, no. 2, pp. 122–130, 2012.
- [2] O. N. Yilmaz, O. Teyeb, and A. Orsino, "Overview of LTE-NR dual connectivity," *IEEE Communications Magazine*, vol. 57, no. 6, pp. 138–144, 2019.
- [3] A. Ghosh, A. Maeder, M. Baker, and D. Chandramouli, "5G evolution: A view on 5G cellular technology beyond 3GPP release 15," *IEEE access*, vol. 7, pp. 127 639–127 651, 2019.
- [4] A. V. Lopez, A. Chervyakov, G. Chance, S. Verma, and Y. Tang, "Opportunities and challenges of mmWave NR," *IEEE Wireless Communications*, vol. 26, no. 2, pp. 4–6, 2019.
- [5] G. Liu, Y. Huang, Z. Chen, L. Liu, Q. Wang, and N. Li, "5G deployment: Standalone vs. Non-standalone from the operator perspective," *IEEE Communications Magazine*, vol. 58, no. 11, pp. 83–89, 2020.
- [6] N. González-Prelcic, A. Ali, V. Va, and R. W. Heath, "Millimeter-wave communication with out-of-band information," *IEEE Communications Magazine*, vol. 55, no. 12, pp. 140–146, 2017.
- [7] M. Hashemi, C. E. Koksall, and N. B. Shroff, "Out-of-band millimeter wave beamforming and communications to achieve low latency and high energy efficiency in 5G systems," *IEEE transactions on communications*, vol. 66, no. 2, pp. 875–888, 2017.
- [8] M. Giordani, M. Polese, A. Roy, D. Castor, and M. Zorzi, "Standalone and non-standalone beam management for 3GPP NR at mmWaves," *IEEE Communications Magazine*, vol. 57, no. 4, pp. 123–129, 2019.
- [9] J. Yang, X. Yang, C.-K. Wen, and S. Jin, "Integrated sensing and communication with multi-domain cooperation," *arXiv preprint arXiv:2105.03065*, 2021.
- [10] 3GPP Technical Report 38.901, "Study on channel model for frequencies from 0.5 to 100 GHz (Release 16)," Dec. 2019.
- [11] R. W. Heath Jr. and A. Lozano, *Foundations of MIMO Communication*. Cambridge University Press, 2018.
- [12] T. S. Rappaport, R. W. Heath Jr., R. C. Daniels, and J. N. Murdock, *Millimeter Wave Wireless Communications*. Pearson Education, 2014.
- [13] K. Stocker, B. Gschwendtner, and F. Landstorfer, "Neural network approach to prediction of terrestrial wave propagation for mobile radio," in *IEE Proceedings H (Microwaves, Antennas and Propagation)*, vol. 140, no. 4, 1993, pp. 315–320.
- [14] P.-R. Chang and W.-H. Yang, "Environment-adaptation mobile radio propagation prediction using radial basis function neural networks," *IEEE Trans. Veh. Techn.*, vol. 46, no. 1, pp. 155–160, 1997.
- [15] L. Bai, C.-X. Wang, J. Huang, Q. Xu, Y. Yang, G. Goussetis, J. Sun, and W. Zhang, "Predicting wireless mmWave massive MIMO channel characteristics using machine learning algorithms," *Wireless Commun. and Mobile Computing*, 2018.
- [16] J. Huang, C.-X. Wang, L. Bai, J. Sun, Y. Yang, J. Li, O. Tirkkonen, and M. Zhou, "A big data enabled channel model for 5G wireless communication systems," *IEEE Trans. Big Data*, vol. 6, no. 2, pp. 211–222, 2018.
- [17] X. Zhao, F. Du, S. Geng, Z. Fu, Z. Wang, Y. Zhang, Z. Zhou, L. Zhang, and L. Yang, "Playback of 5G and beyond measured MIMO channels by an ANN-based modeling and simulation framework," *IEEE J. Sel. Areas Commun.*, vol. 38, no. 9, pp. 1945–1954, 2020.

- [18] W. Xia, S. Rangan, M. Mezzavilla, A. Lozano, G. Geraci, V. Semkin, and G. Loianno, "Millimeter wave channel modeling via generative neural networks," in *Proc. IEEE Globecom Workshops.*, 2020, pp. 1–6.
- [19] V. Degli-Esposti, F. Fuschini, E. M. Vitucci, and G. Falciaesca, "Measurement and modelling of scattering from buildings," *IEEE Transactions on Antennas and Propagation*, vol. 55, no. 1, pp. 143–153, 2007.
- [20] S. Shecklman, L. M. Zurk, S. Henry, and G. P. Kniffin, "Terahertz material detection from diffuse surface scattering," *Journal of Applied Physics*, vol. 109, no. 9, p. 094902, 2011.
- [21] S. Ju, S. H. A. Shah, M. A. Javed, J. Li, G. Palteru, J. Robin, Y. Xing, O. Kanhere, and T. S. Rappaport, "Scattering mechanisms and modeling for terahertz wireless communications," in *ICC 2019-2019 IEEE International Conference on Communications (ICC)*. IEEE, 2019, pp. 1–7.
- [22] Y. Xing and T. S. Rappaport, "Millimeter wave and terahertz urban microcell propagation measurements and models," *IEEE Communications Letters*, vol. 25, no. 12, pp. 3755–3759, 2021.
- [23] J. Huang, C.-X. Wang, H. Chang, J. Sun, and X. Gao, "Multi-frequency multi-scenario millimeter wave MIMO channel measurements and modeling for B5G wireless communication systems," *IEEE Journal on Selected Areas in Communications*, vol. 38, no. 9, pp. 2010–2025, 2020.
- [24] Z. Cui, C. Briso-Rodriguez, K. Guan, Z. Zhong, and F. Quitin, "Multi-frequency air-to-ground channel measurements and analysis for UAV communication systems," *IEEE access*, vol. 8, pp. 110565–110574, 2020.
- [25] W. Khawaja, O. Ozdemir, and I. Guvenc, "UAV Air-to-Ground Channel Characterization for mmWave Systems," in *Proc. IEEE VTC-Fall*, 2017.
- [26] A. Alkhateeb, "DeepMIMO: A generic deep learning dataset for millimeter wave and massive MIMO applications," in *Proc. of Information Theory and Applications Workshop (ITA)*, San Diego, CA, Feb 2019, pp. 1–8.
- [27] "Remcom," available on-line at <https://www.remcom.com/>, 2021-11-11.
- [28] R. He, B. Ai, A. F. Molisch, G. L. Stuber, Q. Li, Z. Zhong, and J. Yu, "Clustering enabled wireless channel modeling using big data algorithms," *IEEE Communications Magazine*, vol. 56, no. 5, pp. 177–183, 2018.
- [29] M. Shafi, A. F. Molisch, P. J. Smith, T. Haustein, P. Zhu, P. De Silva, F. Tufvesson, A. Benjebbour, and G. Wunder, "5G: A Tutorial Overview of Standards, Trials, Challenges, Deployment, and Practice," *IEEE Journal on Selected Areas in Communications*, vol. 35, no. 6, pp. 1201–1221, 2017.
- [30] M. Giordani, M. Polese, M. Mezzavilla, S. Rangan, and M. Zorzi, "Toward 6g networks: Use cases and technologies," *IEEE Communications Magazine*, vol. 58, no. 3, pp. 55–61, 2020.
- [31] T. S. Rappaport, Y. Xing, O. Kanhere, S. Ju, A. Madanayake, S. Mandal, A. Alkhateeb, and G. C. Trichopoulos, "Wireless communications and applications above 100 GHz: Opportunities and challenges for 6G and beyond," *IEEE access*, vol. 7, pp. 78729–78757, 2019.
- [32] P. J. Rousseeuw, "Silhouettes: a graphical aid to the interpretation and validation of cluster analysis," *Journal of computational and applied mathematics*, vol. 20, pp. 53–65, 1987.
- [33] I. Gulrajani, F. Ahmed, M. Arjovsky, V. Dumoulin, and A. Courville, "Improved training of wasserstein gans," *arXiv preprint arXiv:1704.00028*, 2017.
- [34] M. Arjovsky, S. Chintala, and L. Bottou, "Wasserstein generative adversarial networks," in *International conference on machine learning*. PMLR, 2017, pp. 214–223.
- [35] "mmWave channel modeling git hub repository," available on-line at <https://github.com/k1myyaqihu/mmwchanmod-GAN>, 2021-12-14.